PAN
POLISH ACADEMY OF SCIENCES

Opto-Electronics Review

journal homepage: http://journals.pan.pl/opelre

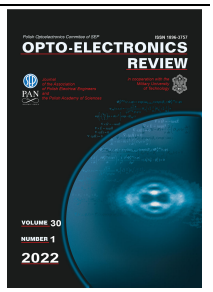

Modelling and analysis of fibre microlenses with ray-tracing and finite-difference methods

Adam Śliwak*, Mateusz Jeleń, Sergiusz Patela

Faculty of Microsystem, Wroclaw University of Science and Technology, ul. Janiszewskiego 11/17, 50-372 Wrocław, Poland

Article info

Article history:
Received 29 Oct. 2021
Received in revised form 27 Nov. 2021
Accepted 14 Dec. 2021
Available on-line: 27 Jan. 2022

Keywords:
Finite-difference time-domain method; knife-edge method; microlens; ray-tracing.

Abstract

Fibre optic microlenses are small optical elements formed on the end-faces of optical fibres. Their dimensions range from a few tens to hundreds of micrometres. In the article, four optical fibre microlenses are modelled and analysed. Microlenses are used for light beam manipulation and quantitative metrics are needed to evaluate the results, for example, the size of focusing spot or intensity distribution. All four lenses tested are made of rods of the same refractive index; they were welded to a single-mode fibre. Two modelling methods were used to analyse the lenses: ray-tracing and finite-difference time-domain. The ray-tracing algorithm moves rays from one plane to another and refracts them on the surfaces. Finite-difference time-domain consists of calculating Maxwell's equations by replacing spatial and temporal derivatives by quotients of finite differences. In this paper, the results of the microlenses analyses obtained from ray-tracing and finite-difference time-domain methods were compared. Both methods of analysis showed the presence of undesirable side lobes related to lens design, namely rods too long for lens fabrication. The test results were compared with the measurements made with the knife-edge method. The use of a single tool to determine parameters of an optical fibre lens does not allow for precise determination of its properties. It is necessary to use different tools and programs. This allows a complete analysis of the beam parameters, letting us find the causes of technical issues that limit the performance of the lenses.

1. Introduction

Today's telecommunication networks are based on optical fibres. One of the main challenges is the interfacing of fibres with optical networking elements, such as routing and multiplexing devices [1]. Photonic integrated circuits (PICs) are usually built with strip waveguides of transverse dimensions below one micrometre, while the diameter of the core of a single-mode fibre equals approximately ten micrometres. Additional elements are required to efficiently couple light between them. These may include tapers on the side of the PIC or micro-optical elements formed on the end-faces of fibres. Fibre end-faces can be in the form of fibre-optic tapers, microlenses, or Fresnel lenses. In this paper, microlenses formed on the end-faces of optical fibres by thermal processing are taken into account. Microlenses provide a useful tool for interfacing optical fibres with photonic devices, such as source, detectors, modulators, and sensors [2].

Depending on the needs, the microlens can collimate or focus light beams emerging from fibres. Obtaining a specific functionality requires the careful lens design.

Design is usually verified by numerical lens modelling, which is an important part of technology development. Modelling can lower the cost of prototyping, shorten time of development, and give better insight into the physical details of the fabricated devices.

There are various numerical tools dedicated to designing and modelling photonic devices. Although they generally claim suitability for any application, their usage is usually slanted towards industry or science. For example,

*Corresponding author at: adam.sliwak@pwr.edu.pl

https://doi.org/10.24425/opelre.2022.140147
1896-3757/ Association of Polish Electrical Engineers (SEP) and Polish Academic of Sciences (PAS). Published by PAS

optical design programs such as OSLO (Lambda Research), ZEMAX (Zemax), SYNOPSYS (Optical Systems Design) or CODE-V (Optical Research Associates) are built for industrial environments. The programs list catalogue components and characterize products in terms of standardized parameters. The calculations are based mainly on sequential ray-tracing algorithms, with Fourier analysis added for diffraction analysis.

When dimensions of the element are within the optical wavelength range, ray-tracing cannot solve the problem, as the assumptions necessary for ray-tracing software are no longer met. Instead, other algorithms are used of which the most popular are the finite-difference time-domain (FDTD) method and the finite-difference beam propagation method (FD-BPM). Physical optics software solves this sort of task, allowing detailed calculations of photonic structures and modelling waveguides and design of both complex structures and singular elements.

For the purpose of the work presented here, the authors used Lumerical (Ansys Inc., Cannonsburg, PA, USA) and OSLO (Lambda Research Corporation, Littleton, MA, USA).

In principle, FDTD can accurately solve any physical optics problem; however, the algorithm is very computationally expensive for 3D structures. For example, the program estimated the time to analyse a 500-µm 3D structure for 20 h a computer with an Intel Core i7-4710MQ processor. Typical dimensional limits for 3D structures are in the range of tenths to hundreds of wavelengths, and larger structures require computers with high calculation power. FD-BPM is less computation-intensive; however, it is best suited for low-index-contrast waveguides, which is not the case here.

The simulations presented there were performed by assuming the axial symmetry of the structure. Since 3D simulations in the above case would not give more accurate results than 2D ones, the authors limited themselves to two-dimensional modelling.

The lens we analysed is made at the end of a single-mode optical fibre; however, it is not created in the optical fibre itself. First, a uniform quartz glass rod is spliced into the fibre. It is only in this rod that the lens is made.

The structure of microlens and physical phenomena that are expected within it are shown in Fig. 1. Light is fed into the lens by a single-mode optical fibre. At the output of the fibre, there is the light intensity distribution LP_{01} in the near-field. It was also assumed that the output light beam diverges in accordance with the value of the fibre numerical aperture [3]. After exiting the optical fibre, the beam propagates in a glass rod with a uniform refractive index. The glass rod functionally forms a multimode waveguide with a high refractive index contrast between glass and air. After the light passes from a single-mode fibre to a multi-mode fibre, a self-imaging effect can be observed. It is a periodic pattern of electromagnetic field distribution reproducing itself along the length of a multimode fibre in the direction of propagation [4].

Capabilities of microlenses make them useful in many areas of life. Due to their small dimensions (less than 1 mm) and low weight, fibre optic microlenses can be used in modern medicine, e.g., as optical scalpels, endoscopes, or optical tweezers [5–7]. They can also serve as illuminators or to destroy cancer tissues with light. Axicon lenses can be used for the coherent tomo-graphy and as components of detectors [2, 8].

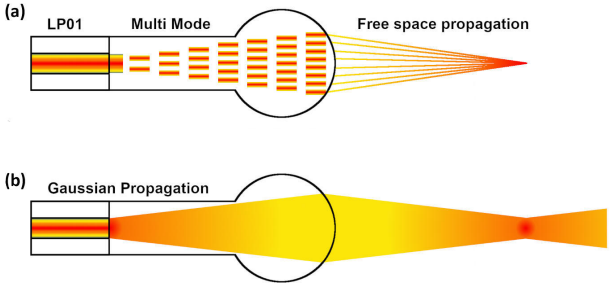

Fig. 1. Schematic of the microlens structure and summary of the phenomena that arise during propagation. Initially, the light is guided by a single-mode fibre. Then, it passes through a short, uniform rod of glass, which is effectively a piece of a multimode waveguide with a high refractive index contrast. The final sphere of glass that forms the lens can be treated as a bulk object through which a beam of light travels in accordance with the laws of optics (a). From the point of view of geometrical optics, a Gaussian beam is propagated through a glass rod-lens optical system (b).

2. Light propagation

Strictly speaking, light is an electromagnetic wave. However, for practical purposes, light is sometimes represented as a beam subject to the laws of refraction and reflection. With this approach, with relative ease, complex lens systems can be designed. The delimitation line is established by the relation of the size of an optical object to the wavelength of light. Optical systems submicrometer size elements cannot be analysed with the ray-tracing approach. In such cases, it is necessary to take into account that light is an electromagnetic wave. The analysis must refer directly to the Maxwell's equations, wave equations, and appropriate boundary conditions.

2.1. Beam characterization

Initially, a laser beam is propagated inside a single-mode fibre which serves as a source of light for the microlens. Inside the fibre, the light distribution takes the form of the fundamental LP_{01} mode. After leaving the fibre, the beam adopts the Gaussian distribution [9]. Advantages of this approach are simplicity of description and availability of well-defined and standardized parameters of beam characterization.

The radius of the Gaussian beam is defined by the distance from the optical axis to the point where the intensity drops to $1/e^2$ of its maximum value [9]. The evolution of the radius with the propagation forms a shape of the beam, visualized in Fig. 2 as a beam envelope. Tangent to the beam envelope creates the angle of the optical axis Θ characterizing the beam divergence. The beam lowest radius is called the beam waist and is marked as w_0. It should be noted that Fig. 2 illustrates a theoretical Gaussian beam. The actual beam will be modified by several factors illustrated in Fig. 1. The beam divergence angle Θ determines by what angle the beam expands moving away from the waist of the beam.

The Rayleigh range determines the beam distance from the waist of the beam to the point where the beam radius

increases by the square root of two. This parameter also determines the location where the beam curvature reaches its maximum; the beam divergence should be measured behind this point. All parameters of the Gaussian beam are illustrated in Fig. 2.

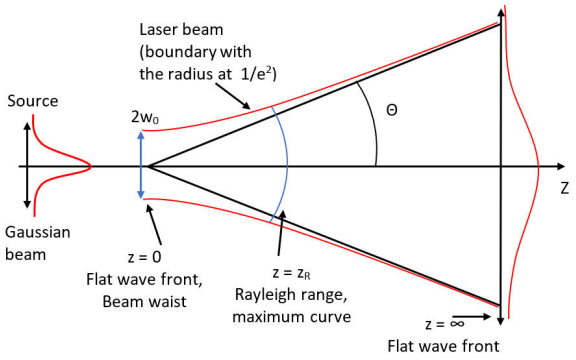

Fig. 2. Parameters of the Gaussian beam and beam evolution with the propagation distance [9].

In Gaussian beams, the formula for the relation of the divergence angle Θ and the radius of the beam waist w_0 is [10]:

$$\Theta \cdot w_0 = \frac{\lambda}{\pi} \tag{1}$$

In the case of real optical beams, this formula also includes the so-called M^2 parameter. This parameter numerically describes the quality of the actual Gaussian beam in comparison to the theoretical one, so that the relation between the angle Θ and the radius w_0 is presented as [10]:

$$\Theta \cdot w_0 = M^2 \cdot \frac{\lambda}{\pi} \tag{2}$$

2.2. Lens performance and beam parameters

To evaluate lens quality and its suitability for a specific application, quantitative metrics are needed to assess lens performance.

Lens design programs offer several such metrics [9, 11]. Due to their simplicity, popularity, and suitability for the evaluation of laser beams, the following four parameters: spot diagram and spot size, encircled energy, radial energy distribution, and M^2 were selected [11].

The spot diagram is a collection of ray points resulting from tracing many rays from a single-point object through the lens aperture. The spot diagram does not necessarily represent distribution of irradiance in the image, as the plot does not show any weighting of the rays. Only in cases where the pupil is uniformly illuminated and rays are uniformly distributed in the pupil, density of the ray intersection in the scatter spot is proportional to the irradiance [11]. The spot size, which usually accompanies a spot diagram, provides the $1/e^2$-beam radius for the X and Y directions.

Encircled energy quantifies the percentage of energy contained in a circle of a specified diameter. It is possible to define the spot size as a circle that contains the specified percentage of beam energy. Calculations can be based on beam geometry (a spot diagram) or diffraction (the spread function) [11]. Radial energy distribution is a function that calculates the radius in which a given percentage of energy is located.

M^2 is a popular parameter that specifies how many times the diameter of an actual beam is larger than the diameter of a perfect Gaussian beam [10].

2.3. Fabrication and structure of microlenses

The microlenses analysed in this work are shaped similarly to commercial lenses, e.g., those manufactured by the Fibrain company (Zaczernie, Poland) [12].

Microlenses are created by fusion with a glass rod to a single-mode fibre and for placing a lens on the end-face of the rod. (It is possible to create the microlens from the fibre itself; however, in this case, the centre area of the lens is an uncontrollable mixture of the fibre core and cladding materials.)

After the rod is connected to the fibre, the lens is formed by thermal heating of the front part of the glass rod.

In this study, the lenses were marked with two parameters: the lens diameter $D = 2R$, where R is the radius and D is the diameter; and the length of the glass rod L, described as the length from the tip of the fibre to the centre of the lens. Four microlenses were examined, all with diameters of 350 µm and rod lengths from 1250 µm to 2000 µm (Fig. 1). Dimensions of the lenses (Fig. 3) were measured with a Leica DM 4000 M LED optical microscope (Leica Microsystems, Wetzlar, Germany). The measured dimension values differ from those provided by the manufacturer. Differences in dimensions can change the calculated focal length and the measured values, so taking authors' own measurements allowed for more accurate lens modelling.

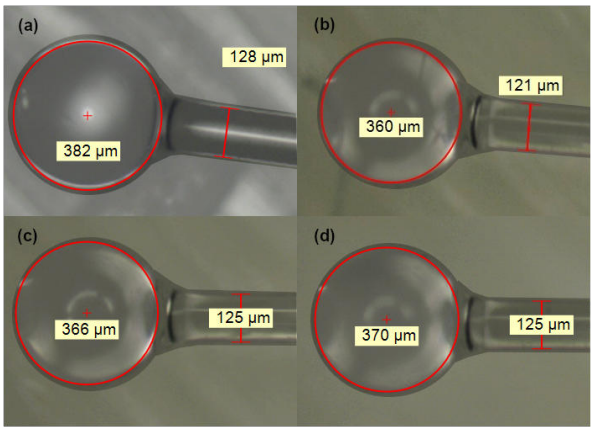

Fig. 3. Photographs of fibre microlenses: 350/1250 (a); 350/1500 (b); 350/1750 (c); 350/2000 (d). The labels inside each lens indicate its diameter.

It should be noted that the patterns visible in Fig. 3 are the result of transformation of optical beams by the observed structure and optics of the microscope; they are not real features. In the analysed structures, the splices were not visible, and authors did not expect any noticeable influence of the splice on the focusing properties of the beam. The dark lines in Fig. 3 are optical artefacts, not splices; thus, splices are not present in the analysis and in Fig. 5 (section 4.1).

3. Modelling tools

3.1. Ray-tracing calculations

The simulations described in the following section were performed with OSLO software and the calculations were based on the ray-tracing algorithm (RTA). Microlens models were created in OSLO software, and then, ray-tracing simulations were performed. Simultaneously, the Gaussian beam parameters were simulated.

The ray-tracing algorithm used is based on the translation of rays from one surface to the next. The rays are refracted on each surface, starting on the surface of the object, and ending on the surface of the image. The translation step computes the intersection of a line and a surface, while the refraction is computed according to Snell's law [1].

3.2. Finite-difference analysis

For finite-difference modelling, the structure, along with the fibre connected to the lens, was modelled using a Lumerical FDTD software. FDTD method replaces spatial and time derivatives in Maxwell's equations with fractions of finite differences. The method allows for the observation of a propagated electromagnetic wave over time. Initially, the modelled area is divided into cells that are as small as possible. The smaller the cell size, the greater the accuracy of the calculations. The wave is then entered into the structure at a time point set by the user, and then, the new field components are calculated based on the differences calculated in the previous iteration [13, 14].

4. Results of the analysis

Dimensions of the lenses were identical in both methods of the analysis. The parameters of the modelled lenses are shown in Table 1. The geometry of the structure included a spherical lens of a given diameter, and a rod of a variable length and a fixed diameter of 125 µm. The length of the rod varies depending on the structure being tested.

Table 1.
Dimensions of the structures of different lenses.

Lens	Length of the rod L [µm]	Lens diameter φ [µm]
350/1250	1059	382
350/1500	1309	382
350/1750	1559	382
350/2000	1809	382

4.1. FDTD modelling

Simulations below were performed using the FDTD module of the Lumerical program. The modelled objects, consisting of a sphere and a rod, were made of silica SiO_2. The pigtail of the SMF-28 fibre optic was attached to the rod. Modelling was performed for a wavelength of 1550 nm which corresponds to the third optical communication window.

Figure 4 shows the entire layout modelled in the FDTD program. Modelling starts with creating a lens with specific dimensions and material parameters. The light source type and the wavelength are then specified. The next step is selecting the modelling area within which the calculation will be performed. Within that area, a grid is added to perform numerical calculations. The next step is selection of the numerical boundary conditions for the modelling area. Choosing the right boundary conditions has a significant impact on the simulation result. Finally, the area from which the data will be collected using the so-called monitors is specified. Modelling area is marked with an orange frame. The area dimensions are of 400×3100 µm. Two monitors were used to record the simulation results. One monitor is about the size of the entire modelling area and the other is depicted as a yellow box (Fig. 4).

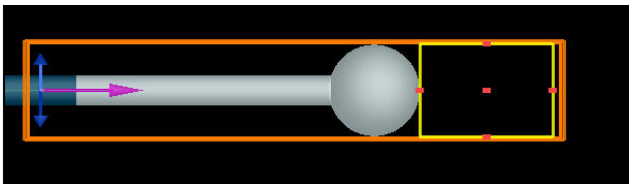

Fig. 4. Modelling area diagram for microlens of 350/1250. The orange frame depicts the modelling area. The yellow frame specifies the monitor from which data is collected.

Figure 5 shows beam intensity distributions throughout the lens, from the source to the end of the modelling area. The lenses described above focus the beam. FDTD simulations show how rays coming out of the source propagate and how intensity is distributed along the propagation path of the structure. The colours in the figure illustrate the power from the lowest intensity (blue) to the highest intensity (red). Lens outlines have also been added to the diagrams. Lenses on the diagrams are elliptical because the X- and Y-axis scales are different.

The wave leaving the single-mode fibre propagates and spreads out in a 125-µm rod. When the beam exits the fibre and enters the rod, there is a self-imaging effect [4] in the rod which acts as a multimode fibre.

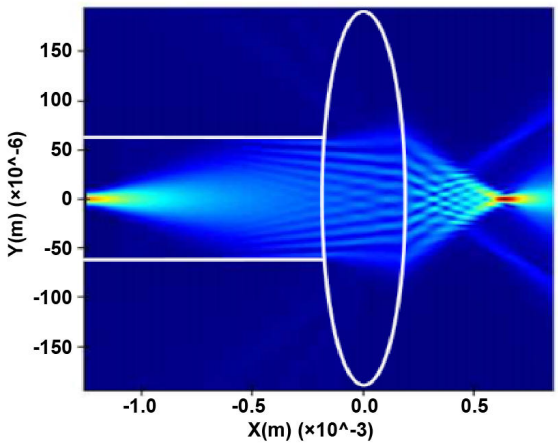

Fig. 5. Simulation results for microlens of 350/1250 and 1510-µm light. The light line shows the lens outline. The outline is elliptical because of different scales of the X- and Y-axis.

Figure 6 shows more precisely the area of waves coming from the structure of the investigated lenses. In this area, the beam envelope and waist can be seen. Also, waves deviating significantly from main rays due to reflections inside the rod could be observed. As the length of the rod attached to the lens increases, the energy transported by rays deviating from the main beam also increases. There is a shift of side-rays towards the focus which can be also seen. With a short rod, rays are far from the focus [Fig. 6(a)]; in Figs. 6(b) and 6(c), they are approaching the focus; in Fig. 6(d), they are very close to the waist of the beam. The energy in the lens that has the shortest rod [Fig. 6(a)] accumulates within and just before the lens focus. As the rod length increases, the area with the highest energy is shortened. The lens with the longest rod [Fig. 6(d)] is characterized by a greater energy transported by side-rays. Furthermore, the high-intensity area around the waist is smaller than in other lenses tested. Compared to other lenses, the self-imaging effect is also more pronounced.

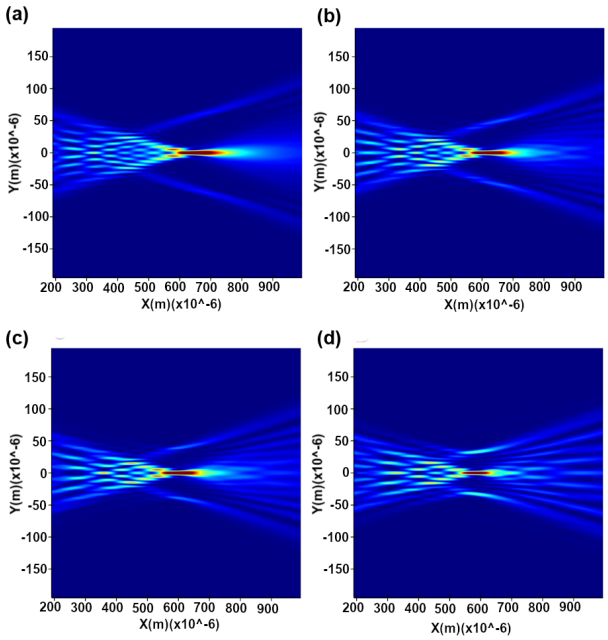

Fig. 6. Comparison of beam intensity graphs for waves leaving lenses: 350/1250 (a); 350/1500 (b); 350/1750 (c); 350/2000 (d).

5. Ray-tracing modelling

The next stage of the study was to analyse the same lens structures with the ray-tracing program (OSLO).

Designing an optical structure involves adding consecutive layers while specifying their thickness and boundary surface radius. For each layer the material must be specified, along with the refractive index or reflective capabilities. Next, parameters of the light beam that will propagate in the structure so that it is consistent with our requirements should be determined.

Figure 7 shows a diagram of the modelled layout. The first block on the left, referred to as an object (OBJ), represents the source of the Gaussian beam; in this case, it is the end-face of the single-mode fibre core.

The second block is a glass rod of a set length. Then, there is the working layer (no. 3) which has a radius equal

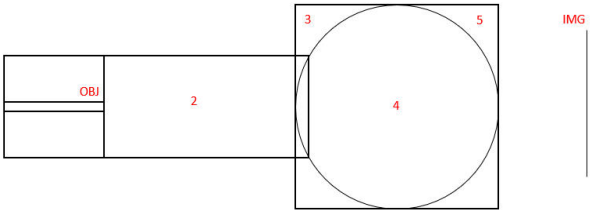

Fig. 7. Software lens model block by block, as described in the text.

to the radius of the lens; it is responsible for the indentation in the end-face of the rod, allowing the rod to merge with the lens. Block number 4 is a glass half-sphere connected to the rod. Block number 5 represents the curvature of the lens output face. The last block of the model is a screen (imaging surface); the block sets the distance from the lens output face to the plane of interest (measuring plane).

Dimensions of the lenses investigated are presented in Table 1 and correspond to the measured dimensions of the lenses tested. The glass (FCA63-65) used in the simulation has parameters similar to those of the actual lenses (refection coefficient and dispersion).

The Gaussian beam envelope was determined using the “spot size” function.

A macro was written that used the spot sizes calculated along the axis. It was observed that the modelled shape of the beam and the placement of the waist differed from the ones measured with the knife-edge measurements. The distance from lens tip to waist on lens of 350/1250, for example, was measured as 0.55 mm, while the simulation indicated 0.23 mm (Fig. 8).

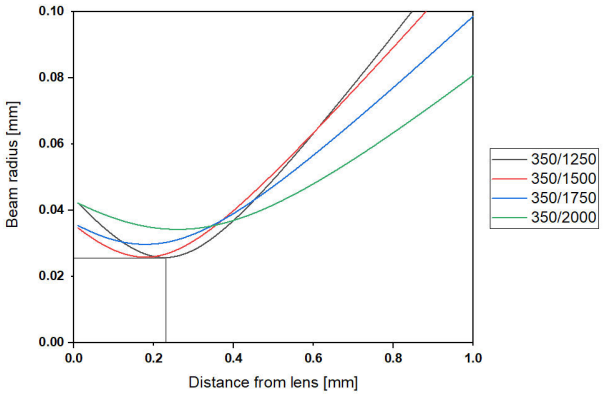

Fig. 8. Combination of envelopes of the beams established by the “spot size” function for lenses from the 350 family.

The observations of shapes of the beams coming out of the lenses led to the conclusion that the “spot size” function is not reliable for calculating the radius of the waist of the beam. Figure 9 shows side lobes that significantly influence the calculations. At this point, it can be also noticed that there are reflections inside the intermediate rod connecting the fibre and the lens. These reflections are responsible for the side lobes. Instead of using the “spot size” function, the spatial energy distributions for the beams formed by the lenses were calculated. Then, values of the beam radius by a circle within which a certain percentage of energy accumulates were determined.

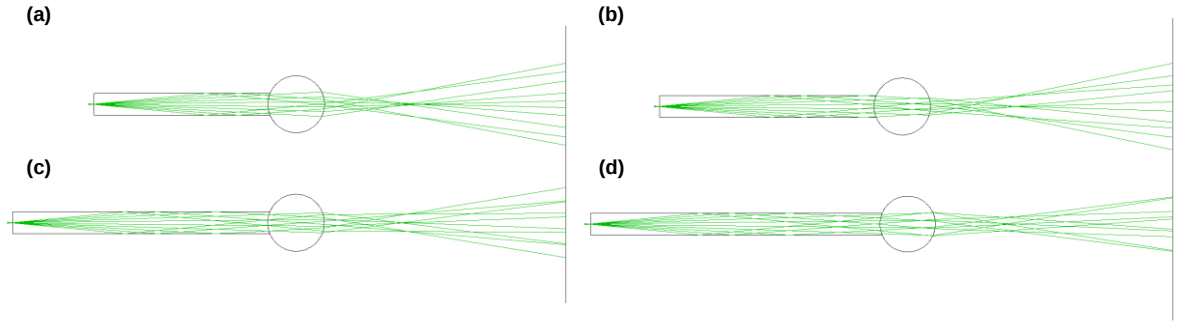

Fig. 9. Comparison of beam shapes for lenses: 350/1250 (a); 350/1500 (b); 350/1750 (c); 350/2000 (d).

In order to calculate the spatial energy distribution of beams formed by the microlenses, the radial energy distribution function was used, which allowed to define the shape of the beam for different energy thresholds. This meant that for a specific threshold value, the envelope of the beam was gathering an exact amount of relative energy. It was observed that the shape of the envelope depends on the threshold established. Figure 9 shows the results of these calculations. The example of 350/1250 microlens for thresholds over 50% [Fig. 10(a)] shows there is only one waist, at a distance of 0.3 mm. However, for thresholds under 50%, the curvature has two minimums, one closer to and one further from the lens tip. Furthermore, in places where curves >50% graphs have their minima, curves <50% have their local maxima.

In the 350/1500 lens shown in Fig. 10(b), the curves are divided into two groups. In one of them (10% and 20%), the curves have two minima in the range studied. This means that only a part of the energy is concentrated close to the optical axis. In subsequent lenses, this effect is magnified [Fig. 10(c) and Fig. 10(d)]. Owing to internal reflections in the rod, only part of the energy (10%) remains close to the optical axis.

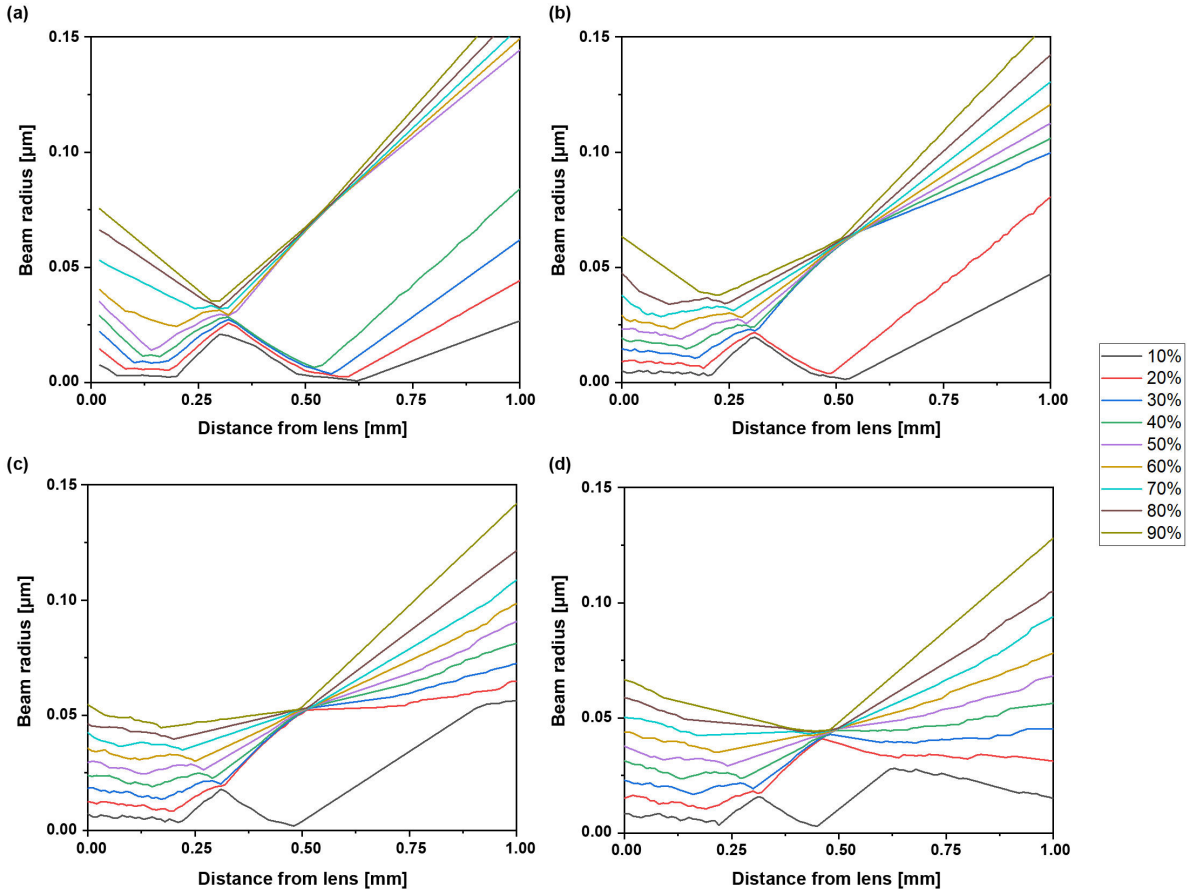

Fig. 10. Graphs of dependence of the beam radius, in which a given percentage of energy is accumulated along the propagation distance in the system: 350/1250 (a), 350/1500 (b), 350/1750 (c), and 350/2000 (d), all calculated with radial energy distribution.

In Fig. 11, ray distributions are shown for the 350/1250 lens; the lower part of the pictures shows how the energy is distributed after leaving the lens.

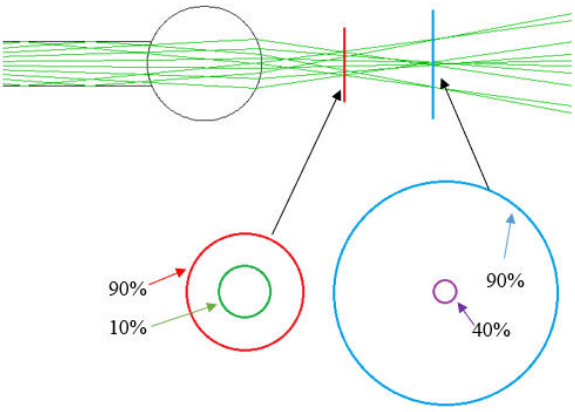

Fig. 11. Comparison of surfaces collecting specific amounts of beam energy for the 350/1250 lens. The red circle represents 90% of the energy collected in the waist of the beam; the green circle shows the area where 10% is concentrated. The blue and purple circles represent the energy distribution and the plane where the smallest focal point is observed; the blue and purple circles represent 90% and 40% of the energy, respectively.

As shown in Fig. 11, the lens exhibits the effect of double focusing. The effect is a result of a total internal reflection of part of the rays which takes place inside the glass rod. Reflected rays and unperturbed rays enter the lens at different angles. They are concentrated at different distances from the main part of the beam. As a result, the energy is distributed, two focal points are observed, and the waist of the beam is displaced relative to the lens. The effect can be eliminated by keeping the intermediate rod length short enough.

According to Fig. 12, the formula that describes the relationship between the maximum length of the glass rod (L), its diameter ($2H$), and the parameters of the optical fibre (NA – numerical aperture, n – refractive index) is:

$$L_{max} = \frac{H_{rod}}{\mathrm{tg}\left(\arcsin\left(\frac{NA}{n}\right)\right)} \tag{3}$$

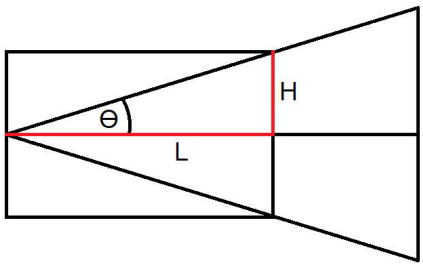

Fig. 12. Diagram of calculation of the critical length of the intermediate glass rod. Below the critical length, the double-focusing effect is not present. In the figure, H stands for the radius of the rod, L is the distance from the optical fibre, and Θ is the beam propagation angle.

With this formula, the critical length of the rod for the microlenses examined was calculated; for a rod with a thickness of 125 µm it should be less than 700 µm. Models with glass rods 25 µm shorter (675 µm) and 25 µm longer (350/725 µm) were then simulated, as shown in Fig. 13.

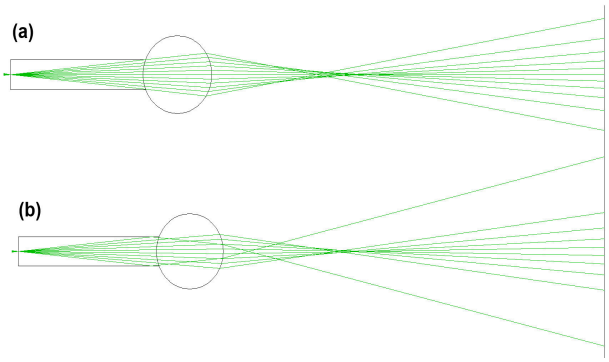

Fig. 13. Comparison of optical beams formed by systems with rod lengths of 675 µm (a) and 725 µm (b). The diameter of the lens is equal to 350 µm.

On the charts of beam envelopes presented in Fig. 14, it can be seen that a structure with a glass rod length below the critical length has a waist that is 4 times narrower. In addition, no side lobes were observed.

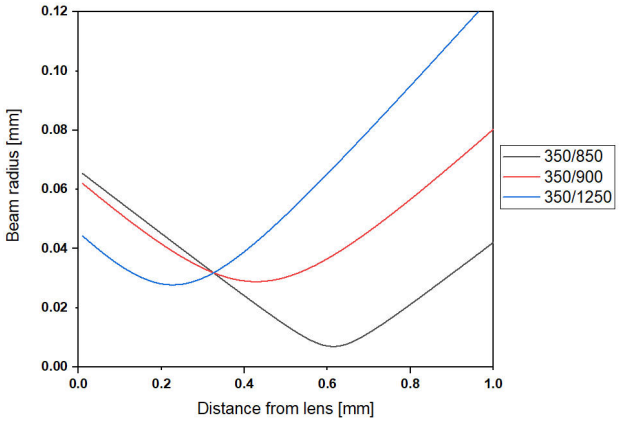

Fig. 14. Comparison of beam envelopes, obtained with the "spot size" function.

Calculations made for the 350/850 lens show that shortening of the intermediate rod improves focusing abilities, as well as energy distribution in the beam. Figure 15 shows that after the reflections in the

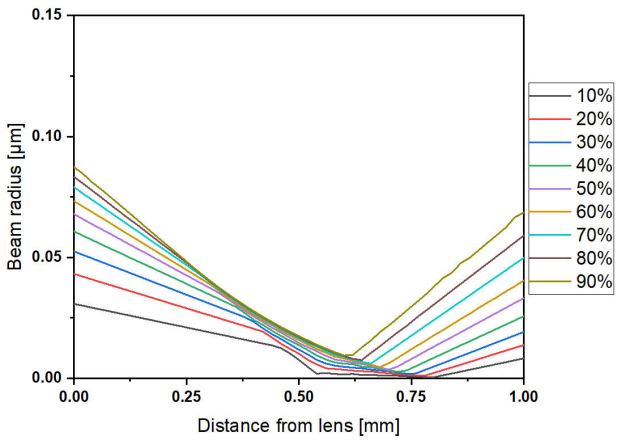

Fig. 15. Diagram of calculated beam radius *vs.* distance from the 350/850 lens, calculated with the radial energy distribution function.

intermediate rod have been eliminated, no side lobes are formed. All the energy is concentrated close to the optical axis. The results correlate well with the calculations performed with the "spot size" function. The location of the focus obtained for the 90% energy threshold and the focus obtained with the "spot size" function are the same.

6. Lens measurement

Measurements were made using the knife-edge method [15]. This method consists of the gradual blocking of the beam coming out of the fibre optic lens through a sharp opaque blade. The edge shift occurs on an axis perpendicular to the beam axis.

Figure 16 shows the results of lens measurements with a diameter of 350 µm. Measurements were carried out at different distances from the lens face. When comparing the characteristics, it can be seen that as the measurement plane approaches the focus, the increments of the curves become sharper. The angle of inclination of the curve is the largest in the area of the focus. In Fig. 16(a), the focus is located at a distance of 550 µm from the lens (in pink), in Fig. 16(b) at a distance of 570 µm, in Fig. 16(c) at a distance of 550 µm, and in Fig. 16(d) at a distance of 450 µm. All the curves are in turquoise.

Differences in results may be due to differences in the length of intermediate rods. Additionally, the lens diameters are not identical, as mentioned in section 2.3. This causes discrepancies in the measurement results.

7. Comparison of different modelling approaches

The use of tools based on the ray-tracing algorithm only (e.g., OSLO) is not sufficient for studying beams containing side lobes. This is due to the fact that in cases of real imperfect beams, the use of standard functions does not ensure that unambiguous results are obtained. Side lobes formed in the structure being examined disturbed the operation of the "spot size" function. Only a more in-depth analysis performed with the "encircled energy" function allowed to detect the characteristics of the examined beam in detail. The "encircled energy" function returns the radius of a circle for a defined energy threshold.

Comparison of the finite-element method with ray-tracing calculations shows that ray-tracking analysis is hundreds to thousands of times faster, lasting a fraction of a second. Because of this fact, it is possible to make on-the-run changes to the lens design, checking the impact of the design on the final result.

Modelling with FDTD is a time-consuming process. The simulation time for one lens using the FDTD method for one wavelength takes several hours. With an increase in the wavelength range, the calculation time increases to a multiple of several hours. The simulation time and accuracy of the results are greatly influenced by the selection of parameters of the calculation grid. With large computation cell sizes, simulations are faster but more error-prone. Small cell dimensions improve the accuracy

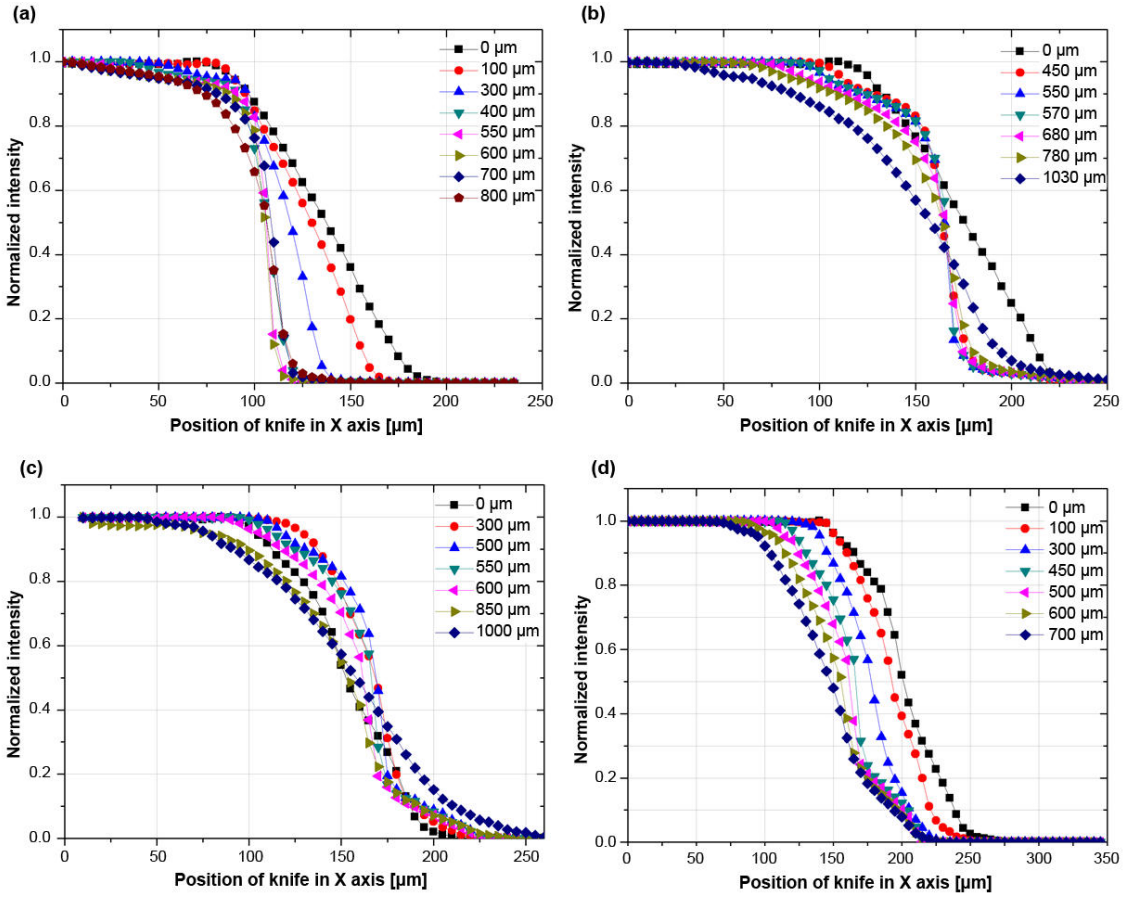

Fig. 16. Results of lens measurements using the knife-edge method: 350/1250 (a), 350/1500 (b), 350/1750 (c), and 350/2000 (d). The curves represent the characteristics of the beam intensity as a function of the position of the blade for different distances from the lens face. The results have been normalized so that they can be compared.

of the simulation but increase its time. For objects of small size (nanometres), simulations are fast (hours), with objects measuring micrometres or millimetres, time is significantly extended. Additional factors determining the results of FDTD simulations are numerical boundary conditions and size of the modelling area. Problems also arise when contact surfaces of subsequent elements of the structure are to be defined. For the modelled structure, it was necessary to determine whether subsequent surfaces should be in contact with each other or combined in another way, e.g., with elements blended into each other. Calculations made in FDTD show the distribution of the beam energy and allow for the calculation of the point with the highest intensity and half-width (FWHM) of the beam.

7. Conclusions

The use of one numeric tool to determine parameters of a fibre optic lens is not enough to obtain the full characteristics of the physical and functional properties of the lens. It is necessary to use at least two tools. This makes it possible to perform a full analysis of the beam parameters and phenomena responsible for the beam formation. Design assumptions underlying the analysis may include requirements for collimation, focussing, and focal spot size.

Design should take into account elements of the microlens manufacturing process. Use of an excessively long lens-forming rod can lead to the appearance of parasitic side lobes that lead to diffusion of the energy in the outgoing beam. Determining the location of the focus simply by determining the location of the beam waist is not reliable, because side lobes distort the results. Additionally, the outgoing beam is distorted by spherical aberrations in the microlens.

Internal reflections in the rod can produce two energy-focusing points. Reflections that change the energy distribution of the beam occur when the beam formed at the output of the optical fibre is too wide to fit the intermediate rod. This means that there is a threshold length of the rod below which that effect does not occur.

Diameter of the rod used in this research was equal to diameter of the optical fibre. It should be noted that a rod with a larger diameter can be used in which case the length for which the parasitic side lobes occur grows.

Performing lens analysis using various numerical tools (ray-tracing, finite-difference analysis) before the lenses are fabricated makes it possible to verify the correctness of design assumptions in terms of the required properties, parameters, and functionality. The ultimate goal of the work will be the optimization of the structures produced. However, the current task was to select and verify the modelling tools. At this stage, authors have focused on changing the length of the rod which significantly affects the operation of the structure and allows to demonstrate the usefulness of modelling. Changing the rod diameter and dimensions of the lens would obscure the image.

References

[1] Tekin, T. Review of packaging of optoelectronic, photonic, and MEMS components. *IEEE J. Sel. Top. Quantum Electron.* **17**, 704–719 (2011). https://doi.org/10.1109/JSTQE.2011.2113171

[2] Zheng, W. Optic Lenses Manufactured on Fibre Ends. in *2015 Optoelectronics Global Conference (OGC)* 1–7 (IEEE, 2015). https://doi.org/10.1109/OGC.2015.7336855

[3] Corning SMF-28 Ultra Optical Fibre. *Corning*. https://www.corning.com/media/worldwide/coc/documents/Fiber/SMF-28%20Ultra.pdf (2014) (Accessed Sept. 3rd, 2021) .

[4] Soldano, L. B. & Pennings, E. C. M. Optical multi-mode interference devices based on self-imaging: principles and applications. *J. Light. Technol.* **13**, 615–627 (1995). https://doi.org/10.1109/50.372474

[5] Yuan, W., Brown, R., Mitzner, W., Yarmus, L. & Li, X. Super-achromatic monolithic microprobe for ultrahigh-resolution endoscopic optical coherence tomography at 800 nm. *Nat. Commun.* **8**, 1531 (2017). https://doi.org/10.1038/s41467-017-01494-4

[6] Liu, Z. L. *et al.* Fabrication and application of a non-contact double-tapered optical fibre tweezers. *Opt. Express* **25**, 22480–22489 (2017). https://doi.org/10.1364/oe.25.022480

[7] Astratov, V. *et al*. *Photonic Nanojets for Laser Surgery*. (SPIE Newsroom, 2010).

[8] Pahlevaninezhad, H. *et al.* Nano-optic endoscope for high-resolution optical coherence tomography in vivo. *Nat. Photonics* **12**, 540–547 (2018). https://doi.org/10.1038/s41566-018-0224-2

[9] Siegman, A. E. *Lasers*. (University Science Books, 1986).

[10] Ross, T. S. *Laser Beam Quality Metrics*. *Laser Beam Quality Metrics* (SPIE, 2013).

[11] *OSLO Optics Software for Layout and Optimization*. *Optics Reference*. (Lambda Research Corporation, Littleton, MA, USA, 2011). https://www.lambdares.com/wp-content/uploads/support/oslo/oslo_edu/oslo-optics-reference.pdf

[12] Fibre Lenses. *Fibrain*. https://photonics.fibrain.com/produkt/fibre-lenses,640.html#zdjecia (2020) (Accessed Aug. 29th, 2020) .

[13] Parsons, J., Burrows, C. P., Sambles, J. R. & Barnes, W. L. A comparison of techniques used to simulate the scattering of electromagnetic radiation by metallic nanostructures. *J. Mod. Opt.* **57**, 356–365 (2010). https://doi.org/10.1080/09500341003628702

[14] Schneider, J. B. *Understanding the Finite-Difference Time-Domain Method*. https://eecs.wsu.edu/~schneidj/ufdtd/ufdtd.pdf (2021).

[15] Bachmann, L., Zezell, D. M. & Maldonado, E. P. Determination of beam width and quality for pulsed lasers using the knife-edge method. *Instrum. Sci. Technol.* **31**, 47–52 (2003). https://doi.org/10.1081/CI-120018406